Research Article GU J Sci, Part A, 10(2): 222-231 (2023) 10.54287/gujsa.1302064

Gazi University
Journal of Science
PART A: ENGINEERING AND INNOVATION
http://dergipark.org.tr/gujsa

The Investigation of CO_2 Gas Sensing Performance of ZnO Nanorods Growth on RF Sputtered Seed Layer

Fatih BULUT[1*] Özgür ÖZTÜRK[2] Selim ACAR[3]

[1]*Sinop University, Scientific and Technological Research Application and Research Center, Sinop, Türkiye*
[2]*Kastamonu University, Department of Electrical and Electronics Engineering, Kastamonu, Türkiye*
[3]*Gazi University, Faculty of Science, Department of Physics, Science Faculty, Ankara, Türkiye*

Keywords

Zinc Oxide
Nanorod
Hydrothermal
CO_2 Gas Sensor
Nickel Doping

Abstract

In this study, one-dimensional ZnO nanorod structures with different ratios of nickel doping were produced using the hydrothermal method. The presence of nickel doping in different ratios caused variations in the fundamental characteristics of the nanorods that grew on the RF sputtered seed layer, such as crystallinity quality, morphology, diameter of the nanorods, band gap energy, resistance of the sample, and CO_2 gas sensing. Produced samples were found to form like hexagonal rods and crystallize in a wurtzite structure, and the ratio of nickel doping improved the crystallin quality and the morphology of sample surface. This study showed that the 5% nickel doped sample provided the most effective results in sensing CO_2 gas at different concentrations. Overall, the study provided valuable insights into the relationship between doping system and the basic characteristics of wurtzite-type hexagonal ZnO.

Cite

Bulut, F., Öztürk, Ö., & Acar, S. (2023). The Investigation of CO_2 Gas Sensing Performance of ZnO Nanorods Growth on RF Sputtered Seed Layer. *GU J Sci, Part A, 10*(2), 222-231. doi:10.54287/gujsa.1302064

Author ID (ORCID Number)

0000-0001-5335-2307 Fatih BULUT
0000-0002-0391-5551 Özgür ÖZTÜRK
0000-0003-4014-7800 Selim ACAR

Article Process

Submission Date 24.05.2023
Revision Date 10.06.2023
Accepted Date 16.06.2023
Published Date 23.06.2023

1. INTRODUCTION

Sensors have greatly improved our lives and made things easier by providing information to machines and processors in response to changes in the environment. They come in various types and serve different purposes, like regulating temperature in our homes or determining fuel levels in our vehicles (Jagadale et al., 2018). Sensors can convert chemical or physical quantities into electrical signals using different stimuli, such as heat, light, pressure, force, electricity, and distance. The investigating and developing of air quality and gas sensors has become increasingly essential in addressing global warming and air pollution (K. Xu et al., 2018). Carbon dioxide (CO_2) gas sensing is particularly relevant due to its role in the greenhouse gas effect. ZnO-based semiconductor sensors are commonly used in this field due to their low cost, non-toxicity, and modifiable selectivity and sensing properties through dopant elements (Mirzaei et al., 2016). However, these sensors have drawbacks including insufficient stability, inadequate response, and high operating temperature, which researchers address through doping or changes in production techniques (Cai et al., 2023). Researchers have explored various ZnO-based nanomaterial structures, such as nanorods, nanowires, and nanoparticles, to improve gas sensing properties. One-dimensional (1D) orientation and surface morphology are preferable for enhancing gas sensing properties, as they increase the surface area (Zhang et al., 2018). Additionally, the electronic performance of one-dimensional zinc oxide nanostructures is critical in electronic applications, and element doping is another means of improving sensing properties (Saini et al., 2022; Wan et al., 2022). Kamble et al. (2021) has reported in 2021 that 2% Ni-doped ZnO sensor responded at its maximum level of 356% to NO_2 gas at a concentration of 100 ppm at operating temperature of 200°C.

*Corresponding Author, e-mail: fatihbulut@sinop.edu.tr

M. Xu et al. (2014) state that nickel doped zinc oxide nanorods were created using quick microwave hydrothermal synthesis, and their enhanced gas-sensing performance was demonstrated in the work. The sensitivity of the produced samples based on nickel doped zinc oxide NRs was up to 313 at 500 ppm ethanol environment. (M. Xu et al., 2014). Abdel All et al. (2021) reported that nickel doped zinc oxide nanoparticles were used as the functional material for CO_2 gas sensors. The data collected at 350°C showed an improvement in the sensor's sensitivity to CO_2.

In the current study, zinc oxide nanorods doped with nickel were produced on an RF-sputtered seed layer by hydrothermal method in 1D orientation. In addition to their structural, morphological, and optical properties, 1D oriented nanorods exhibit CO_2 gas sensing capabilities were investigated.

2. MATERIAL AND METHOD

RF sputtering at 150°C temperature and 10mTorr chamber pressure were applied for coating ZnO seed layer on glass substrate. RF sputtering power set to 75W, and substrate rotated by 10 rpm during sputtering, and sputtered glass substrates were annealed at 600°C for half hour. Doped and undoped ZnO nanorods were produced by hydrothermally on seed layer at 90°C for 3 hours. In 50 mL DI water, we mixed 0.1 M Zn Acetate dehydrate and hexamethylenetetramine (HMTA, $C_6H_{12}N_4$) to prepare hydrothermal solutions. For the doping process, they added the required amount of doping elements (1, 3 and 5%wt) to the same solution. These solutions were then used in a hydrothermal process to grow nanorods on seed layer-coated substrates, which were placed in a Teflon autoclave. After production prosses at 90°C for 3 hours, samples were rinsed using DI water and dried at 50°C (Bulut et al., 2022).

Bruker D8 Advance powder X-ray diffractometer, FEI Quanta FEG 250 SEM, Shimadzu 2600 UV-Spectrometer are used to measure phase purities, surface morphology, optical properties of produced samples. Gas sensing properties of produced samples investigated by homemade gas sensing system which has MKS series mass flow controllers, LakeShore 325 temperature controller and Keitheley 2400 DC sourcemeter.

3. RESULTS AND DISCUSSION

XRD results of undoped, and nickel doped samples have given in Figure 1. All samples have single (002) peak which is responsible for c axis growing (Galioglu et al., 2018; Bura et al., 2022). The peak in Figure 1 is supports that crystals have grown in c axis and resulted as nanorod. In the diffraction patterns, no contaminants or secondary phases like Ni or NiO were seen. The effective insertion of Ni ions into the Zn sites in the crystal structure is responsible for the absence of any secondary phases. By using Warren-Sheerer equation c lattice parameter of all samples have been calculated and listed in Table1 (Galioglu et al., 2018; Bulut et al., 2022). By increasing of the Ni doping ratio in the ZnO system, c lattice parameters tended to decrease while the crystal size increased. The incorporation of dopant particles into ZnO materials affects their lattice cell parameters by creating unique strain fields within the crystal structure. These interactions also produce variations in energy levels, leading to significant changes in the c lattice cell parameter (Bulut et al., 2022).

SEM images of the sample were taken at 1μm scaled and given in Figure 2. SEM images are important to see the surface of the produced material, grain boundaries, measuring grain size and also having information about the surface morphology of the samples. Nanorods grown on an RF-sputtered seed layer exhibit perfect hexagonal symmetry and the nanorods were perpendicular to the substrate, as demonstrated via Figure 2. Calculated NR average diameter values are given in Table 1 as nm and it is clear that Ni doping ratio effected the NR average diameter. Minimum NR average diameter measured for 1Ni sample as 61.21nm. It is to be mentioned here that generally the doping ratio increases the nanorod diameter. In addition, the varying ionic radii (IoRad) of dopant elements ($IoRad_{Zn^{+2}} = 0.72Å$, $IoRad_{Ni^{+2}} = 0.69Å$) may be depend on the diameters changes.

Basically, the band gap which can be calculated via the transmittance–wavelength graph taken from UV-Spectrophotometer, is the parameter to having knowledge of the conductivity of the samples produced. The band gap values of the samples given in Table1 and represented in Figure 3. enhancing of the doping ratio

caused the decreasing of E_g values which may attributed to having closer atomic radios of Zn^{+2} (0.72Å) and Ni^{+2} (0.69Å) (Singh et al., 2017). According to the table, the highest E_g of the pure sample is calculated as 3.26 eV, is consistent with ZnO nanorod values in the literature. In addition, Table 1 demonstrates that the band gap energy decreases monotonically with increasing dopant concentration. This is due to the band-shrinkage effect brought about by the increase in concentration of the carriers. In addition, the inhomogeneity of the interfacial charges, the different diameters of the nanorods grown, the composition and thickness of the ZnO oxide layer all play key role in the reduction of the E_g values.

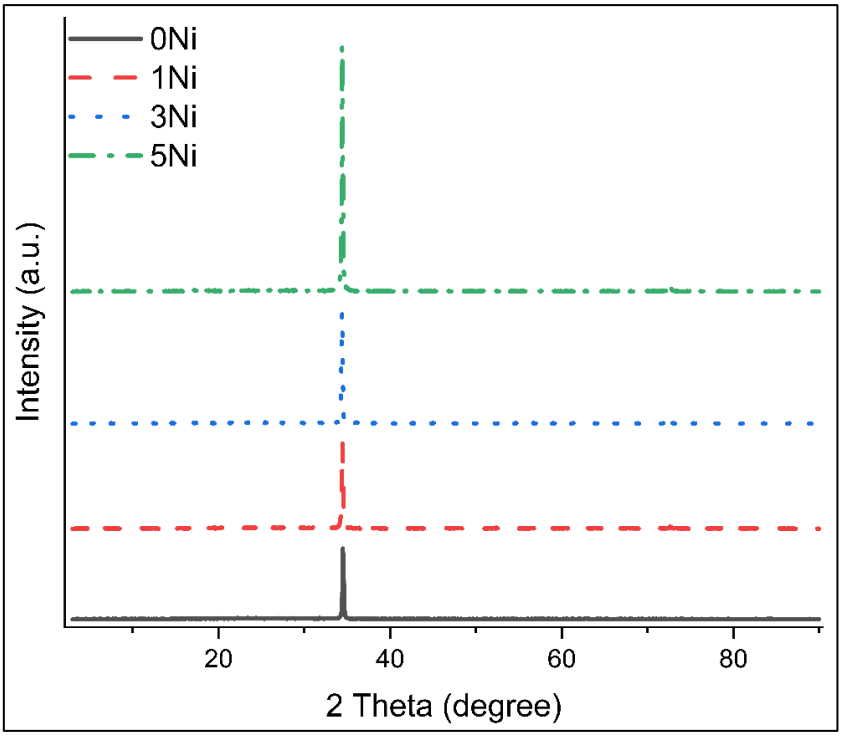

Figure 1. *XRD results of produced samples*

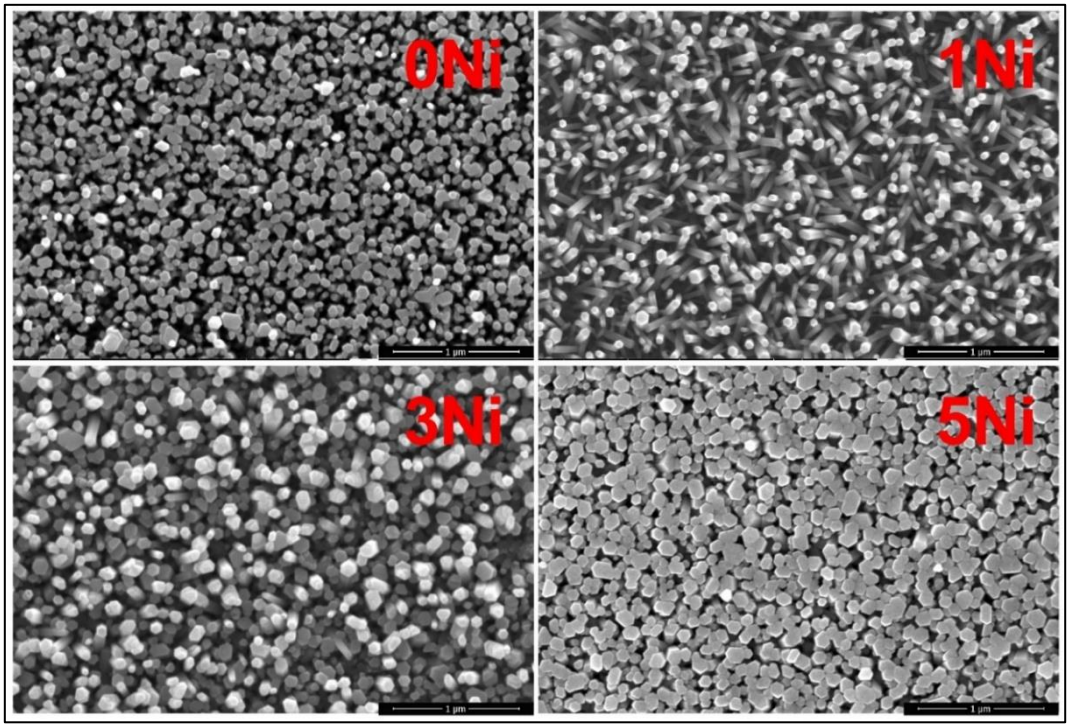

Figure 2. *SEM images of produced samples*

Table 1. *The parameters such as crystallite size (D), c lattice parameter, average diameter and band gap calculated from XRD, SEM and optical analysis*

Sample Name	D (nm)	c (Å)	Average Diameter of NRs (nm)	E_g (eV)
0Ni	36.49	5.209	72.91	3.23
1Ni	41.27	5.205	61.21	3.19
3Ni	45.72	5.202	73.84	3.11
5Ni	49.13	5.197	77.36	3.08

Metal oxide materials offer a technique for gas detection based on the chemical reactions that happen between the gas molecules and the surface of the MO. Due to its ability to grab an electron in the metal oxide's conductivity band (CB) and stick to the surface, oxygen's chemical absorption plays a major part in sensing process.

Sensor materials use a surface-controlled method for sensing, with adsorption/desorption process of the O_2 on the outside layer of sensor. At low temperatures, on the sensor's surface, O_2 molecules are adsorbed, which traps valence band electrons. At higher temperatures, O_2 molecules separate into active species that are negatively charged. CO_2 gas combines with the oxygen species that adsorbed by surface, lowering the resistance. When CO_2 gas was introduced to the ZnO sensor, the deposited O ions reacted with the gas to remove the electrons from the CB of n-type zinc oxide sensor (Eqs.1 & 2). As a result, there were less electrons present on sensor's surface, and the sensor resistance increased (Anderson et al., 2009; Kannan et al., 2014).

$$CO_{2(g)} + e^- \rightarrow CO^-_{2(adsorbed)} \quad (1)$$

$$CO_{2(adsorbed)} + O_{2(adsorbed)} + 2e^- \rightarrow CO_g + 2O^{2-}_{(adsorbed)} \quad (2)$$

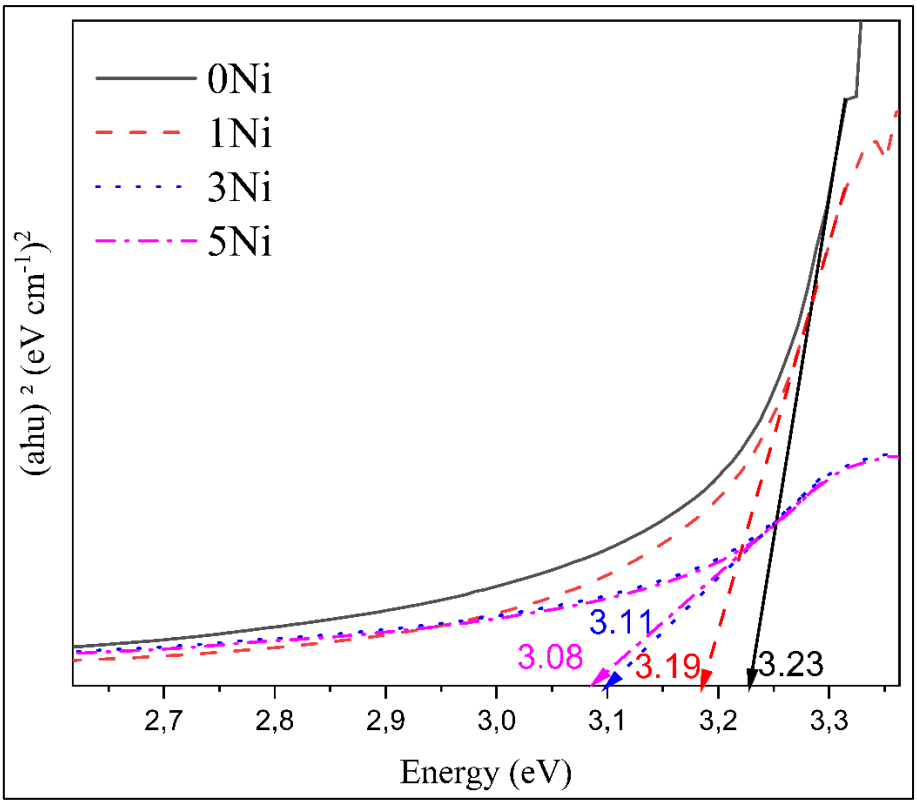

Figure 3. *Band gap graph of produced samples*

Sensing response (S) is one of the important parameters for the gas sensors like response end recovery times (Barin et al., 2022). For the chemiresistive gas sensors, calculating sensing response is depending on the resistance measurement under air and target gas atmosphere. To identify the optimum operating/sensing temperature, resistance measurement of the sensors performed for 50ppm CO_2 gas. Because of the oxidizing nature of CO_2 gas, the interaction with sensors returns as increasing resistance. This circumstance is explained by the restricted mobility of the charge carrier. In addition, it should be mentioned, nickel doped ZnO sensors have significantly higher sensor resistance value. That situation attributed to the properties of the optical band gap and the crystal structure (Saxena et al., 2020; Ocak et al., 2021). Sensing response values were calculated using the Eq.3 given below,

$$S = \frac{\Delta R}{R_a} = \frac{|R_a - R_g|}{R_a} \tag{3}$$

In Eq3, while S is the sensing response, Ra–Rg represents the resistance values of the sensor under air–gas atmosphere, respectively. Calculated S values are represented in the Figure 4. Increasing of the sensing response values under CO_2 gas atmosphere were clearly visible from the Figure 4 and that is the characteristic behavior of the semiconductor which are categorized as n type sensor under oxidizing gas (Wisitsoraat et al., 2009). The increasing of the sensing temperature also enhanced the sensing responses of produced sensors. The optimum temperature was determined as 420K of the sensors except for the 5Ni sample and, for 5Ni, the working temperature is 400K. While 1Ni has the highest sensing response at 420K, 5Ni has the lowest.

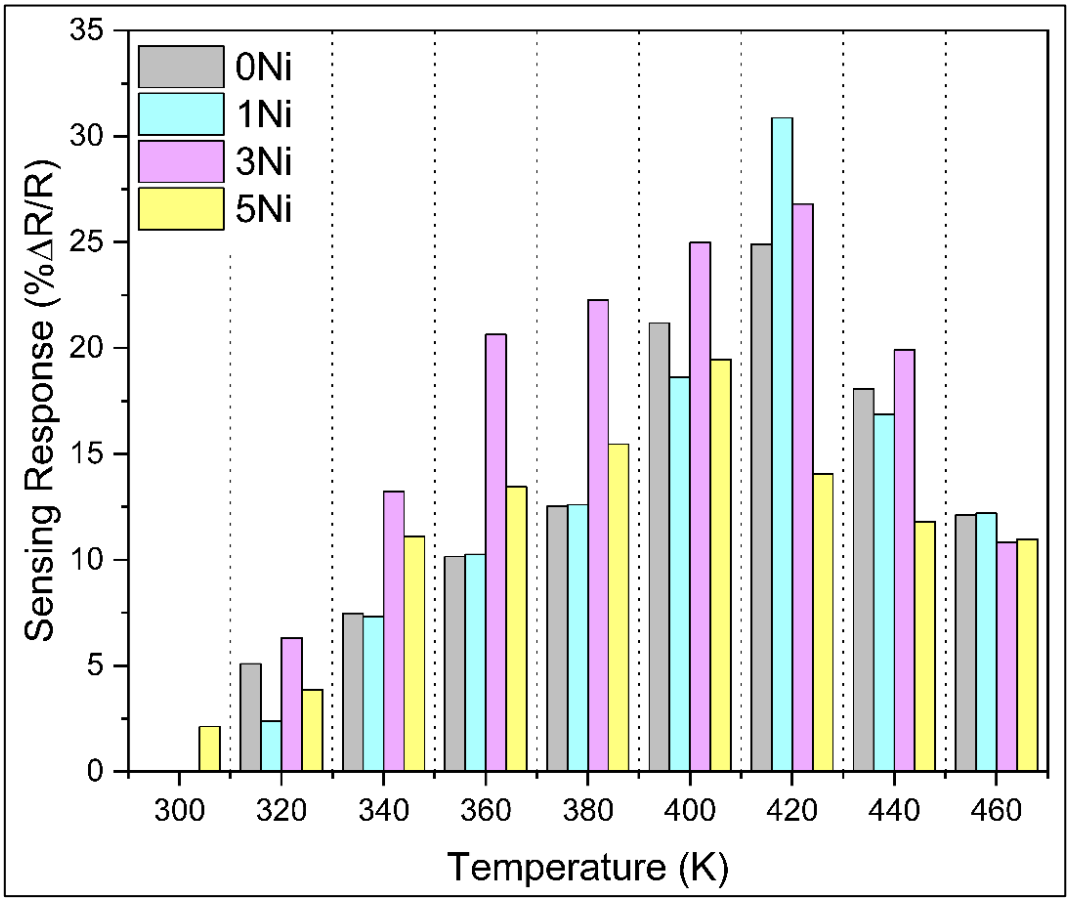

Figure 4. *Calculated response of the sensors at different temperatures*

After determining the working temperatures, the sensors are exposed to different concentrations of gas at these temperatures (Figure 5). In this way, the selectivity of the sensors for a CO_2 is examined, and the result are given in Figure 6. By enhancing of the gas concentration exposure of the gas sensor, resistance of the produced sensors was increased. Nickel doped ZnO sensors' resistance levels under gas atmosphere are

shown to grow progressively with increasing CO_2 content, according to experimental data. It is evident that the doping ratio influences sensor behavior. While 5Ni sensor has given the lowest value at 50ppm CO_2 in different temperatures, it represented the highest CO_2 sensing response at 100ppm CO_2. With sufficient spacing between the rods, more surface-target gas interaction is provided for the 1Ni sample. The CO_2 gas may not be able to reach every spot because of the 5Ni sensor restricted surface and bigger nanorod diameters. While 1Ni shows the best CO_2 detection performance at different concentrations, the 3Ni sample comes in second in this field. However, when the surface morphologies are investigated, it is understood that the 3Ni sensor's surface is less stable than 1Ni. Although it has hexagonal nanorods on the surface, the 3Ni sensor does not have standardized NRs like the 1Ni sample. Deterioration of NRs on the surface of the 3Ni sensor with 3% Ni doping may have caused a diminish in the CO_2 sensing performance.

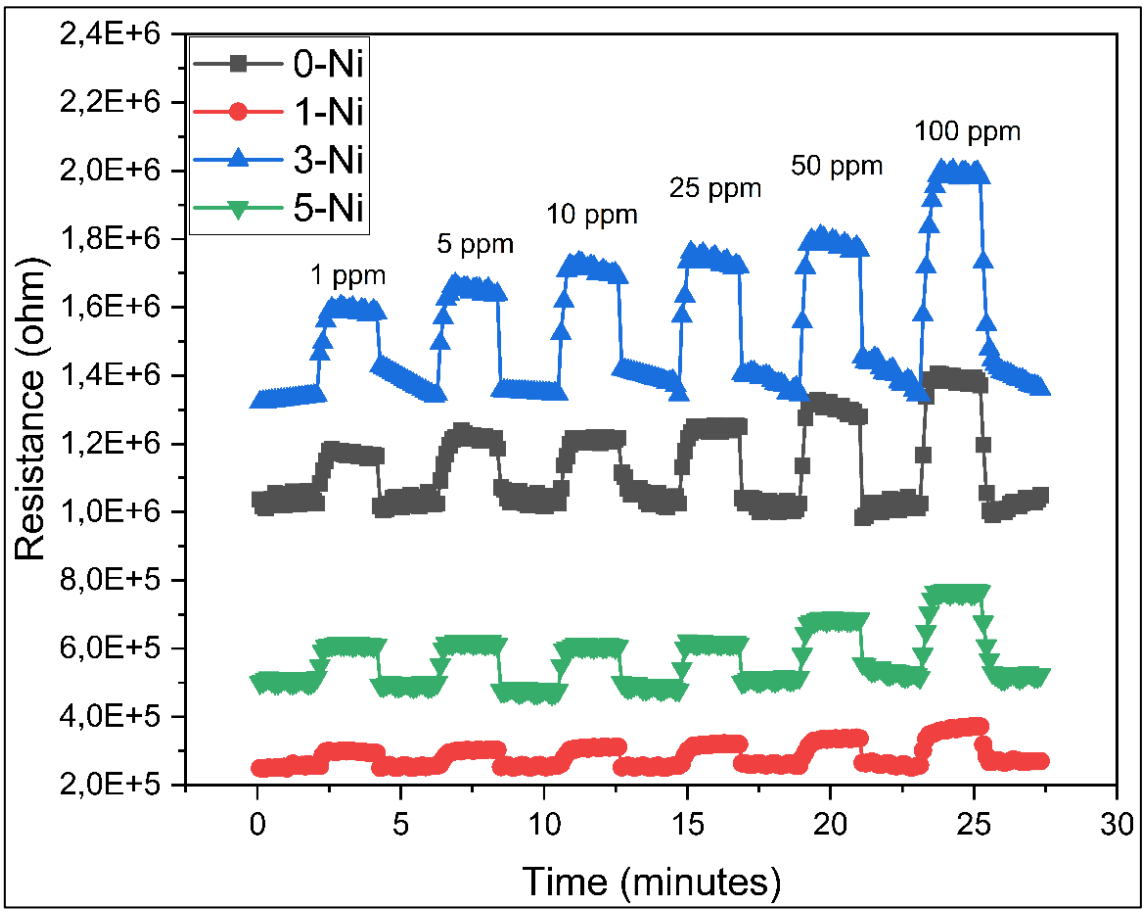

Figure 5. *Resistance vs Time graph of the sensors at different concentrations*

Another key parameter for gas sensors are the response time and the recovery time. Figure 7a and 7b represents the response and recovery times of the sensor produced in this study. Response times of the sensors shows that 1Ni sensor has lower response time among all sensors while has nearly faster recovery time. 5N sensor gives the highest recovery time. Surface morphology of the sensors given in the Figure 2 may support the recovery times of the sensors. It is seen from the SEM images of the 5Ni sensor that the surface density is high. This causes a decrease in the gap between the NRs. If the gap between the NRs is small, it is seen that the recovery time value is high. This interpretation is supported when Figure 2 and Figure 7 are evaluated together. Accordingly, the recovery time values of the 1Ni sensor, where NRs are rare, are quite low compared to the 5Ni sensor.

In the wurtzite crystal structure, local p-n junctions form when nickel ions aren't replaced by zinc ions, according to experimental observations published in the scientific literature (Cho et al., 2015). As a result, as mentioned in the literature (Kar & Kamilla, 2021), instead of Schottky barriers, p-n junctions could control the sensor's response. The data obtained in this study are compared with the literature in Table 2, where the ZnO structures produced for gas sensing. As known the sensor's response is influenced by the surface area,

and 1Ni has more NRs that are perpendicular to the surface. Comparing the reactions of Ni-doped sensors at 500K and 50 ppm CO_2, it is evident that 1Ni exhibits greater sensitivity than the other due to its larger surface area.

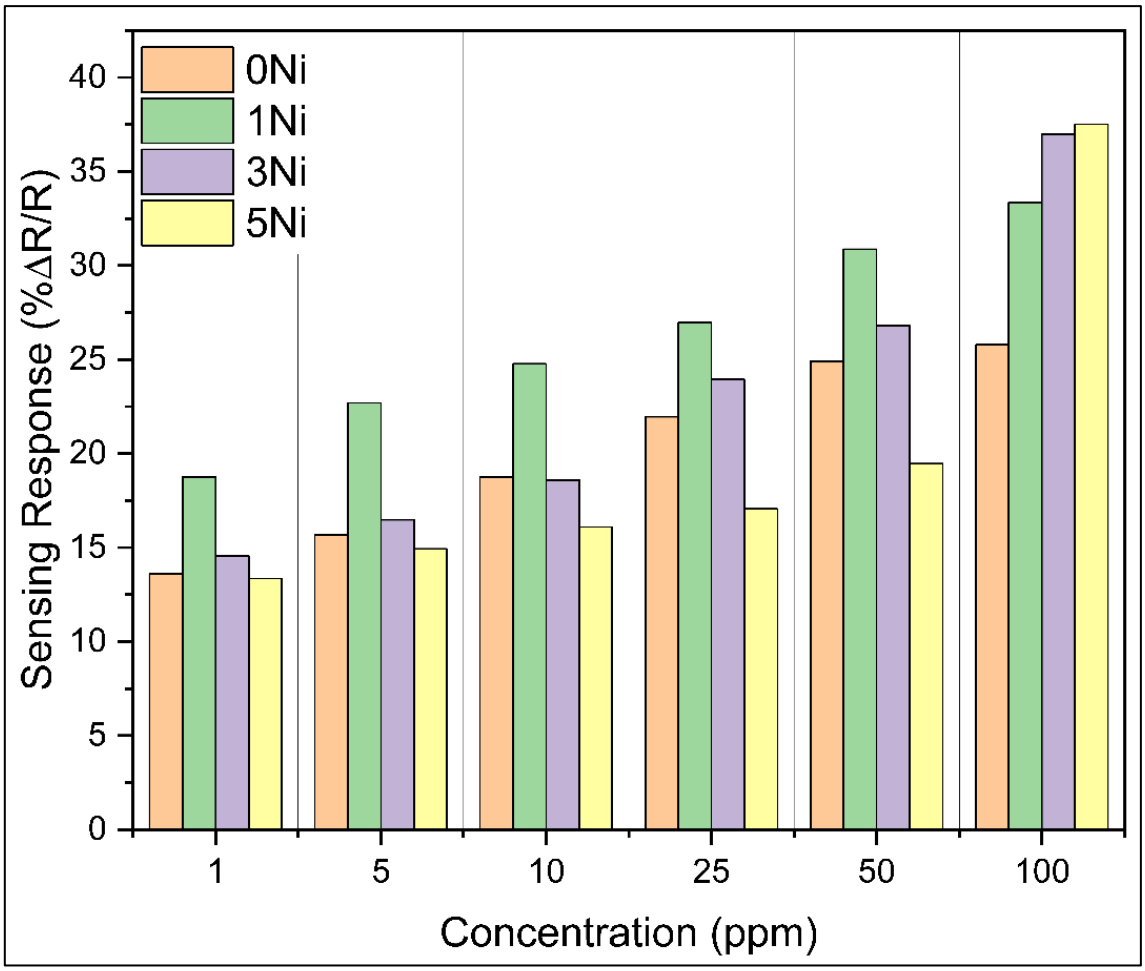

Figure 6. *Calculated response of the sensors at different CO_2 gas concentrations*

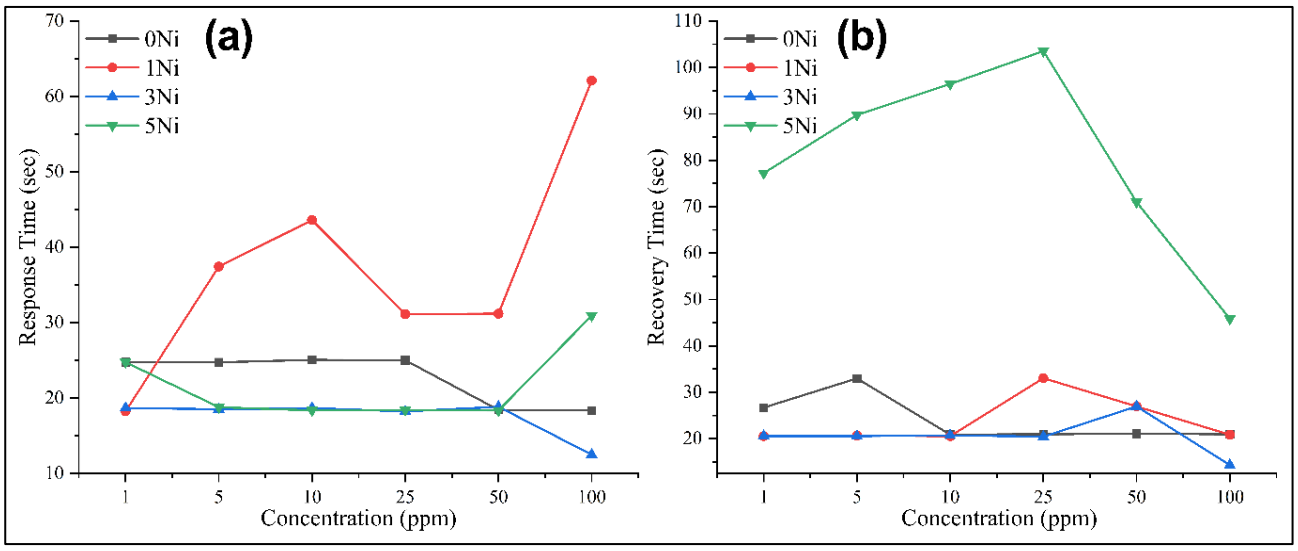

Figure 7. *Calculated; **a)** response and **b)** recovery times of produced sensors*

Table 2. *Summarized results for CO_2 gas sensing properties*

Doping and Host Material	Method/Production	Working Temperature (Kelvin)	Target Gas Concentration (ppm)	% Sensing Response
Ni-doped ZnO nanorods (M. Xu et al., 2014)	Fast microwave hydrothermal	643	500	313
ZnO Nanoflowers (Kanaparthi & Singh, 2019)	Precipitation (Simple method)	520	200	23
ZnO Nanoparticles, Al doped (Dhahri et al., 2017)	Sol-Gel thin film	520	10000	100
ZnO loaded %50La (Jeong et al., 2016)	Hydrothermal	670	5000	65
5Ni (this study)	Hydrothermal	500	100	37.5

4. CONCLUSION

By doping Ni at different ratios, ZnO nanorods were hydrothermally produced on the RF sputtered ZnO seed layers. The growth of ZnO nanorods doped with Ni in various ratios was accomplished using RF sputtered ZnO seed layers. A single (002) peak was found when the structural properties were examined using XRD analysis. The sample's computed crystalline sizes revealed an increase in crystalline size with higher doping ratios. The surface morphology and typical nanorod properties were examined using SEM. A UV spectrophotometer was used to illuminate the doping effect on band gap values and show how doping causes a drop in the band gap value. The 0Ni, 1Ni, and 3Ni samples all showed higher reaction rates at 420K, while the 5Ni sample showed a response rate at 400K. After figuring out the operating temperatures, the sensing performance of the samples at various CO_2 concentrations was evaluated. For the 1Ni sensor, higher response rates at various concentrations were seen. The sensors' response and recovery times were calculated. For various concentrations, the sensors with smaller nanorod diameters displayed faster response times. In contrast to other sensors, the 1Ni sensor featured a sparse structure and a smaller average nanorod diameter. The gas detection capabilities of the zinc oxide NR structure grown on the seed layer made using the RF sputtering method were shown to be enhanced by doping nickel at various concentrations.

CONFLICT OF INTEREST

The authors declare no conflict of interest.

REFERENCES

Abdel All, N., El Ghoul, J., & Khouqeer, G. (2021). Synthesis and Characterization of Ni-Doped ZnO Nanoparticles for CO_2 Gas Sensing. *Journal of Nanoelectronics and Optoelectronics*, *16*(11), 1762-1768. doi:10.1166/jno.2021.3121

Anderson, T., Ren, F., Pearton, S., Kang, B. S., Wang, H.-T., Chang, C.-Y., & Lin, J. (2009). Advances in Hydrogen, Carbon Dioxide, and Hydrocarbon Gas Sensor Technology Using GaN and ZnO-Based Devices. *Sensors*, *9*(6), 4669-4694. doi:10.3390/s90604669

Barin, Ö., Ajjaq, A., Çağırtekin, A. O., Karaduman Er, I., Yıldırım, M. A., Ateş, A., & Acar, S. (2022). Pivotal role of nucleation layers in the hydrothermally-assisted growth of ZnO and its H2 gas sensing performance. *Sensors and Actuators B: Chemical*, *371*, 132499. doi:10.1016/j.snb.2022.132499

Bulut, F., Ozturk, Ö., Acar, S., & Yildirim, G. (2022). Effect of Ni and Al doping on structural, optical, and CO_2 gas sensing properties of 1D ZnO nanorods produced by hydrothermal method. *Microscopy Research and Technique*, *85*(4), 1502-1517. doi:10.1002/jemt.24013

Bura, M., Singh, G., Gupta, D., Malik, N., Salim, A., Kumar, A., Singhal, R., Kumar, S., & Aggarwal, S. (2022). Transition in the preferred orientation of RF sputtered ZnO/Si thin films by thermal annealing:

Structural, morphological, and optical characteristics. *Optical Materials*, *133*, 113024. doi:10.1016/j.optmat.2022.113024

Cai, Z., Park, J., & Park, S. (2023). Synergistic effect of Pd and Fe_2O_3 nanoparticles embedded in porous NiO nanofibers on hydrogen gas detection: Fabrication, characterization, and sensing mechanism exploration. *Sensors and Actuators B: Chemical*, *388*, 133836. doi:10.1016/j.snb.2023.133836

Cho, Y. H., Liang, X., Kang, Y. C., & Lee, J.-H. (2015). Ultrasensitive detection of trimethylamine using Rh-doped SnO_2 hollow spheres prepared by ultrasonic spray pyrolysis. *Sensors and Actuators, B: Chemical*, *207*(Part A), 330-337. doi:10.1016/j.snb.2014.10.001

Dhahri, R., Leonardi, S. G., Hjiri, M., Mir, L. E., Bonavita, A., Donato, N., Iannazzo, D., & Neri, G. (2017). Enhanced performance of novel calcium/aluminum co-doped zinc oxide for CO_2 sensors. *Sensors and Actuators B: Chemical*, *239*, 36-44. doi:10.1016/j.snb.2016.07.155

Galioglu, S., Karaduman, I., Çorlu, T., Akata, B., Yıldırım, M. A., Ateş, A., & Acar, S. (2018). Zeolite A coated $Zn_{1-X}Cu_XO$ MOS sensors for NO gas detection. *Journal of Materials Science: Materials in Electronics*, *29*(2), 1356-1368. doi:10.1007/s10854-017-8042-8

Jagadale, S. B., Patil, V. L., Vanalakar, S. A., Patil, P. S., & Deshmukh, H. P. (2018). Preparation, characterization of 1D ZnO nanorods and their gas sensing properties. *Ceramics International*, *44*(3), 3333-3340. doi:10.1016/j.ceramint.2017.11.116

Jeong, Y.-J., Balamurugan, C., & Lee, D.-W. (2016). Enhanced CO2 gas-sensing performance of ZnO nanopowder by La loaded during simple hydrothermal method. *Sensors and Actuators B: Chemical*, *229*, 288-296. doi:10.1016/j.snb.2015.11.093

Kamble, V. S., Navale, Y. H., Patil, V. B., Desai, N. K., & Salunkhe, S. T. (2021). Enhanced NO2 gas sensing performance of Ni-doped ZnO nanostructures. *Journal of Materials Science: Materials in Electronics*, *32*(2), 2219-2233. doi:10.1007/s10854-020-04987-z

Kanaparthi, S., & Singh, S. G. (2019). Chemiresistive Sensor Based on Zinc Oxide Nanoflakes for CO_2 Detection. *ACS Applied Nano Materials*, *2*(2), 700-706. doi:10.1021/acsanm.8b01763

Kannan, P. K., Saraswathi, R., & Rayappan, J. B. B. (2014). CO_2 gas sensing properties of DC reactive magnetron sputtered ZnO thin film. *Ceramics International*, *40*(8, Part B), 13115-13122. doi:10.1016/j.ceramint.2014.05.011

Kar, N., & Kamilla, S. K. (2021, October 8-10). Performance of Ni-doped ZnO nanoparticles towards CH3-CO-CH3 sensing. In: N. Nayak, T. Parida, T. P. Dash, L. M. Satpathy, M. Mishra, M. Sahani, D. A. Gadnayak, & S. Coudhury (Eds.), Proceedings of the International Conference in Advances in Power, Signal, and Information Technology (APSIT), Bhubaneswar, India. doi:10.1109/APSIT52773.2021.9641451

Mirzaei, A., Park, S., Kheel, H., Sun, G.-J., Lee, S., & Lee, C. (2016). ZnO-capped nanorod gas sensors. *Ceramics International*, *42*(5), 6187-6197. doi:10.1016/j.ceramint.2015.12.179

Ocak, Y. S., Zeggar, M. L., Genişel, M. F., Uzun, N. U., & Aida, M. S. (2021). CO_2 sensing behavior of vertically aligned Si Nanowire/ZnO structures. *Materials Science in Semiconductor Processing*, *134*, 106028. doi:10.1016/j.mssp.2021.106028

Saini, S., Kumar, A., Ranwa, S., & Tyagi, A. K. (2022). Highly sensitive NO_2 gas sensor based on Ag decorated ZnO nanorods. *Applied Physics A*, *128*(5), 454. doi:10.1007/s00339-022-05606-w

Saxena, N., Manzhi, P., Choudhary, R. J., Upadhyay, S., Ojha, S., Umapathy, G. R., Chawla, V., Sinha, O. P., & Krishna, R. (2020). Performance optimization of transparent and conductive Zn1-xAlxO thin films for opto-electronic devices: An experimental & first-principles investigation. *Vacuum*, *177*. doi:10.1016/j.vacuum.2020.109369

Singh, S., Kumar, Y., Kumar, H., Vyas, S., Periasamy, C., Chakrabarti, P., Jit, S., & Park, S.-H. (2017). A study of hydrothermally grown ZnO nanorod-based metal-semiconductor-metal UV detectors on glass substrates. *Nanomaterials and Nanotechnology*, *7*. doi:10.1177/1847980417702144

Wan, M., Shi, C., Qian, X., Qin, Y., Jing, J., Che, H., Ren, F., Li, J., & Yu, B. (2022). Interface assembly of flower-like Ni-MOF functional MXene towards the fire safety of thermoplastic polyurethanes. *Composites Part A: Applied Science and Manufacturing*, *163*, 107187. doi:10.1016/j.compositesa.2022.107187

Wisitsoraat, A., Tuantranont, A., Comini, E., Sberveglieri, G., & Wlodarski, W. (2009). Characterization of n-type and p-type semiconductor gas sensors based on NiO_x doped TiO_2 thin films. *Thin Solid Films*, *517*(8), 2775-2780. doi:10.1016/j.tsf.2008.10.090

Xu, K., Fu, C., Gao, Z., Wei, F., Ying, Y., Xu, C., & Fu, G. (2018). Nanomaterial-based gas sensors: A review. *Instrumentation Science & Technology*, *46*(2), 115-145. doi:10.1080/10739149.2017.1340896

Xu, M., Li, Q., Ma, Y., & Fan, H. (2014). Ni-doped ZnO nanorods gas sensor: Enhanced gas-sensing properties, AC and DC electrical behaviors. *Sensors and Actuators B: Chemical*, *199*, 403-409. doi:10.1016/j.snb.2014.03.108

Zhang, Y., Liu, Y., Zhou, L., Liu, D., Liu, F., Liu, F., Liang, X., Yan, X., Gao, Y., & Lu, G. (2018). The role of Ce doping in enhancing sensing performance of ZnO-based gas sensor by adjusting the proportion of oxygen species. *Sensors and Actuators, B: Chemical*, *273*, 991-998. doi:10.1016/j.snb.2018.05.167